Scientific Research Publishing

Materials Sciences and Applications, 2024, 15, 559-571
https://www.scirp.org/journal/msa
ISSN Online: 2153-1188
ISSN Print: 2153-117X

Zirconium Metal Recovery from Zircaloy in Molten Fluorides

Laurent Massot[1*], Mathieu Gibilaro[1], Delphine Quaranta[1,2], Jerome Serp[2], Pierre Chamelot[1]

[1]Laboratoire de Génie Chimique, Université de Toulouse, Toulouse, France
[2]Université de Montpellier, Marcoule, France
Email: *laurent.massot@univ-tlse3.fr

How to cite this paper: Massot, L., Gibilaro, M., Quaranta, D., Serp, J. and Chamelot, P. (2024) Zirconium Metal Recovery from Zircaloy in Molten Fluorides. *Materials Sciences and Applications*, **15**, 559-571.
https://doi.org/10.4236/msa.2024.1512037

Received: November 14, 2024
Accepted: December 28, 2024
Published: December 31, 2024

Abstract

This article focuses on the electrorefining process in molten fluorides to selectively recover zirconium from one Zr-based metallic alloy involved in the field of nuclear energy: Zircaloy-4. Firstly, zirconium electrodeposition was investigated in molten LiF-NaF at 750˚C in order to determine appropriate operating conditions to ensure Zr metal recovery: concentration and applied current density. Then, anodic behaviour of Zircaloy-4 was studied and compared to its composing elements. These results allowed us to define an adapted electrorefining strategy. Electrorefining progress, anodic and cathodic faradic efficiencies were evaluated by materials characterization obtained after galvanostatic electrolyses.

Keywords

Molten Fluorides, Zirconium, Zircaloy-4, Electrorefining, Dissolution Pathway

1. Introduction

Zirconium is of great interest in the nuclear field due to its interesting physicochemical properties such as low cross-section of neutron capture, corrosion resistance under high temperature and aggressive conditions and great mechanical resistance. Zirconium is used in several forms: bulk metal in dissolvers for spent nuclear fuel reprocessing, alloyed with uranium in U-Zr fuel or with other metals for zirconium alloys claddings (Zircaloy, Zirlo, …) [1]. Consequently, its recovery from these different materials can be considered an attractive option for Zr production. The choice was made to focus on a Zr-based alloy currently used in nuclear fuel field: Zircaloy-4.

This alloy consists in a homogenous metallic phase containing Zr, Sn, Fe and Cr [2] [3]. The main elements composition as well as other elements considered as impurities (*i.e.* concentration lower than 120 ppm) are listed in **Table 1**.

Table 1. Composition of Zircaloy-4.

Main elements	Content/ mass%	Elements (impurities)	Content/ ppm	Elements (impurities)	Content/ ppm
Sn	1.20 - 1.70	Al	75	Mg	20
Fe	0.18 - 0.24	B	0.5	Mn	50
Cr	0.07 - 0.13	Cd	0.5	Mo	50
O	0.09 - 0.16	C	270	Ni	70
Zr	base	Co	20	N	80
		Cu	50	Si	120
		Hf	100	W	100
		H	25	Ti	50

Electrorefining process in high temperature molten salts is a very interesting way to reactive metals recovery such as zirconium from metallic alloys. It was successfully performed in house to recover silicon from solar panels wafers [4]. The objective of the study is to evaluate the feasibility of using an electrorefining process in molten salts for Zr recovery from Zircaloy-4.

Electrochemical behavior of zirconium has been studied in molten chloride and fluoride media [5]-[13]. In molten chlorides, results evidenced the existence of several oxidation states (0, +I, +II and +IV) and different $ZrCl_4$ reduction pathways to metal were proposed. Lee *et al.* [6] proposed a three-step reduction mechanism: $ZrCl_4 \leftrightarrows ZrCl_2 \leftrightarrows ZrCl \leftrightarrows Zr$.

Other studies showed a two-step reduction mechanism implying different redox couples [5] [7] [8]. For the first step, the same reaction was proposed:

$$ZrCl_4 + 2e^- \leftrightarrows ZrCl_2 + 2Cl^- \quad (1)$$

The second step was more discussed and different possibilities were proposed: Ghosh *et al.* proposed a two-electron reduction into metal (see Equation (2)) [5], while Sakamura *et al.* envisaged a combination of two reactions (see Equation (3) and Equation (4)) [7]. Finally, Fabian *et al.* proposed an overall combination of these three reactions [8].

$$ZrCl_2 + 2e^- \leftrightarrows Zr + 2Cl^- \quad (2)$$

$$ZrCl_4 + 4e^- \leftrightarrows Zr + 4Cl^- \quad (3)$$

$$ZrCl_4 + 3e^- \leftrightarrows ZrCl + 3Cl^- \quad (4)$$

In fluoride media, Zr(IV) reduction mechanism into metal seems to be simpler: either a two-step reduction [11] or an one-step reduction [9] [10] [13] was proposed:

$$ZrF_4 + 2e^- \leftrightarrows ZrF_2 + 2F^- \quad (5)$$

$$ZrF_2 + 2e^- \leftrightarrows Zr + 2F^- \quad (6)$$

or

$$ZrF_4 + 4e^- \leftrightarrows Zr + 4F^- \quad (7)$$

Few studies concerning zirconium recovery are described in the bibliography. All studies were conducted in molten LiCl-KCl. Han *et al.* [14] used an iron electrode to produce Zr-Fe alloys from LiCl-KCl-K_2ZrF_6 at 723K with an efficiency of around 98%. Murakami *et al.* [15] performed reductive extraction involving $ZrCl_4$ as an oxidative agent to dissolve transuranium nitride fuels in molten LiCl-KCl. Concerning electrorefining process, Sohn *et al.* [16] carried out Zr recovery with 99.9% purity from radioactively contaminated Zirconium alloys in LiCl-KCl-$ZrCl_4$ medium.

Due to the existence of multiple oxidation states of Zr in molten chlorides, LiF-NaF fluoride medium was chosen in the present work to study Zr electrorefining through the dissolution of Zircaloy-4 anode. The study is divided into two parts: 1) study of zirconium electrodeposition in molten LiF-NaF on different cathodic substrates at 750˚C and 2) evaluation of the overall electrorefining process with SEM-EDS characterizations and anodic and cathodic faradic efficiencies.

2. Experimental

2.1. The Cell

Figure 1 presents the electrochemical set up used in this work, composed of a vitreous carbon crucible (3) placed in a boron nitride secondary crucible (2). The two crucibles were placed in a cylindrical Inconel reactor (1) closed by a lid (4) cooled by air circulation. The experiments were carried out under an inert argon atmosphere (<0.1 ppm O_2 and <0.5 ppm H_2O). The cell was heated using a programmable furnace. The temperature was controlled by a platinum-rhodium thermocouple. This equipment was placed in a glovebox under dry argon atmosphere (<5 ppm O_2 and <2 ppm H_2O).

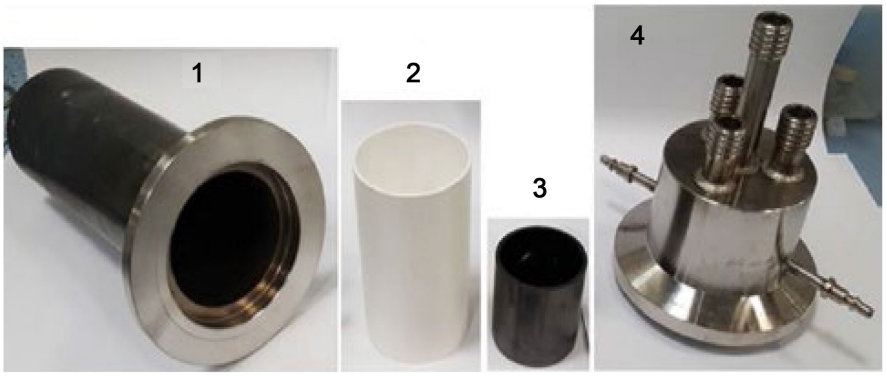

Figure 1. Photographs of the cell (1, 4) and crucibles (2, 3) used for experiments in molten LiF-NaF.

2.2. Chemicals and Electrodes

The electrolytic bath was composed of LiF–NaF (Sigma Aldrich 99.99%) eutectic mixture (60 - 40 mol%). This mixture was initially dehydrated by heating under vacuum (7×10^{-5} bar) from ambient temperature up to its melting point (650˚C) for 70 h. Zirconium ions were added to the bath in the form of zirconium (IV) fluoride ZrF_4 (Alfa Aesar 99.9%).

Zirconium, chromium, iron, niobium, tin, cobalt, nickel wires (1 mm diameter) and Zircaloy-4 rod (3 mm diameter) were used as working electrodes. The surface area of the working electrode was determined by measuring the immersion depth in the salt after each experiment. The counter electrode was a zirconium plate for electrodeposition investigation and a vitreous carbon (3000C) rod (3 mm diameter) for electrorefining process. The potentials were referred to a platinum wire (1 mm diameter) acting as a quasi-reference electrode $Pt/PtO_x/O^{2-}$ [17].

2.3. Electrochemical and Material Characterizations

Transient electrochemical techniques used in this study are cyclic voltammetry, square wave voltammetry and chronoamperometry. Investigations were carried out with a VSP potentiostat/galvanostat controlled with EC-Lab V11.01 software.

The electrode surfaces and cross-sections were characterized by a Scanning Electron Microscope (Phenom XL) coupled with an Energy Dispersive Spectroscopy probe.

ICP-AES (Horiba Ultima 2) was used to analyze the impurities content in the bath after cooling.

2.4. Salt Cleaning Process of Zr Deposits

In order to characterize Zr coatings after electrodeposition runs, it was particularly important to remove the residual salt eventually present at the surface of the electrode. As the solubility of fluoride salts in water is very low, it was decided to immerse the deposits into an ultrasonic cleaner full of pure water for 15 - 20 hours.

The efficiency of this ultrasonic cleaning methodology is shown in **Figure 2** with a Zr deposit on a graphite substrate. All the Zr deposits obtained in this study have been cleaned before observation and characterization.

Figure 2. Typical Zr deposit on graphite cathode (a) before and (b) after ultrasonic cleaning.

3. Results and Discussion

3.1. Zr Recovery Strategy

Electrorefining is an electrochemical method used for metal purification. It consists in oxidizing the material (metal, alloy, …) to be purified at the anode, while depositing a pure metal at the cathode. The main issues to be considered are the electrodeposition conditions at the cathode and the anodic behaviour of the material.

The electrorefining process selectivity depends on the dissolution potentials of the metal to be treated. Considering a material containing zirconium and impurities, if the impurity dissolution potential is higher the Zr one, the impurity is not anodically dissolved. The electrorefining selectivity is thus ensured by the anode potential. On the contrary, if the impurity dissolution potential is lower, the impurity is simultaneously dissolved with zirconium but is not reduced at the cathode. The process selectivity is governed by the cathode potential. Finally, if the dissolution potentials are similar, the impurity is dissolved together with Zr: its electrochemical reduction behaviour has to be studied to evaluate the possibility of its co-deposition with zirconium.

3.2. Zirconium Electrodeposition

The electrochemical behaviour of Zr(IV) species in molten fluorides has been already established in previous studies in our laboratory in molten LiF-CaF_2 by Gibilaro *et al*. [10] and in LiF-NaF by Quaranta *et al*. [13]. The results showed that Zr(IV) is reduced into Zr metal in a diffusion controlled one-step process exchanging four electrons. Quaranta *et al*. [13] also studied the electrocristallization phenomenon and demonstrated that the nucleation mode of Zr electrodeposition process is progressive. To obtain a smooth coating structure, the creation of a high number of nuclei is essential, which is favoured by both high temperature and overvoltage. Nevertheless, for too high overvoltage, the electrolyte diffusion limitation can promote dendritic growth phenomena. Considering these conflicting effects, it was decided to investigate zirconium coatings in different operating conditions by varying Zr(IV) concentration and applied current density. To have the possibility to clearly highlight the influence of these operating conditions, two significantly different values were selected: 0.49 and 1.96 mol·kg^{-1} for Zr(IV) content and an applied current density of −35 and −110 mA·cm^{-2}.

3.2.1. Influence of Zr(IV) Concentration

To evaluate the impact of Zr(IV) content in the solution on the coating morphology, Zr electrodepositions were done on a graphite substrate at −35 mA·cm^{-2} and 750˚C for different Zr(IV) molalities. **Figure 3** shows typical photographs of deposits done at 0.49 and 1.96 mol·kg^{-1}. The surface morphology of the deposits is clearly influenced by Zr(IV) concentration: the roughness of coating realized at high Zr(IV) content is lower than at low Zr(IV) concentration. This observation agrees with the progressive nucleation mode established in our previous study

[13]: higher solute concentration leads to a higher germination rate, so a greater number of generated nuclei, improving the coating compacity.

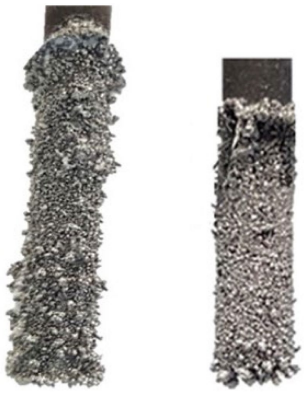

Figure 3. Photographs of Zr deposits on graphite substrate at −0.035 A·cm^{-2} for 5 h in LiF-NaF-ZrF_4 at 750˚C for 0.49 (a) and 1.96 (b) mol·kg^{-1} of Zr(IV).

3.2.2. Influence of the Applied Current Density

The influence of the applied current density on the Zr deposits morphology can be observed in **Figure 4**, for two electrolyses performed at −35 (a) and −100 (b) mA·cm^{-2} on graphite electrode at 750˚C and Zr(IV) molality of 1.96 mol·kg^{-1}. This figure clearly highlights that at high current density, coatings become dendritic and thus have a high roughness. This result has already been observed in previous studies concerning silicon, tantalum and niobium electrodeposition in molten fluorides [18]-[20] and is also in agreement with a progressive nucleation mode. It can be noted that the applied current density has a greater impact on the morphology than the Zr(IV) concentration. The dendritic aspect of Zr deposits should not be problematic since they are adherent enough to the substrate to prevent any loss of Zr metal into the melt.

Figure 4. Photographs of Zr deposits on graphite substrate in LiF-NaF-ZrF_4 (1.96 mol·kg^{-1}) at 750˚C at two current densities: −35 (a) and −110 (b) mA·cm^{-2}.

These results conclude that Zr recovery by electrodeposition can be efficient during long durations electrolyses with a applied current density of around −0.1 A·cm^{-2} on graphite electrode.

3.3. Zircaloy-4 Anodic Behaviour

As mentioned in the introduction part, Zircaloy-4 is a Zr-based alloy mainly containing Cr, Fe and Sn (cf. Table 1). In order to confirm the alloy homogeneity, a SEM micrograph of a cross-section is presented in Figure 5: Zircaloy-4 is a single-phase material with homogeneous composition.

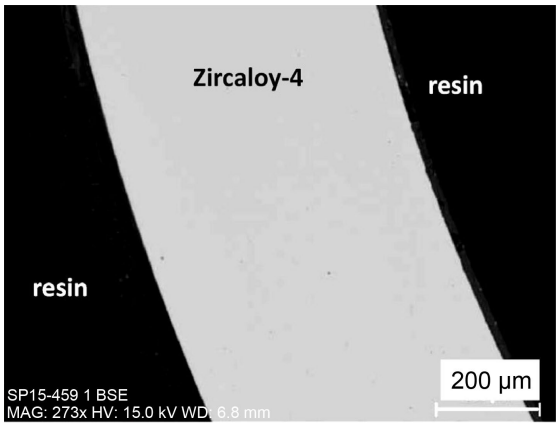

Figure 5. SEM micrograph of Zircaloy-4 cross-section.

The anodic behaviour of Zircaloy-4 was compared to those of Zr and several metals considered as impurities in LiF-NaF at 750˚C by linear sweep voltammetry at 10 mV·s^{-1}.

The plots for Zircaloy-4, Zr, Cr, Nb, Fe, Sn, Co and Ni are shown in Figure 6. As it can be observed, the anodic behaviour of Zircaloy-4 and Zr is similar, with the same dissolution potential and an oxidation rate slightly lowered for Zircaloy-4. Finally, Figure 6 also highlights that Cr, Fe, Nb, Sn, Co and Ni are anodically dissolved at a higher potential than Zr: the selective dissolution of Zr from Zircaloy-4 is thus possible.

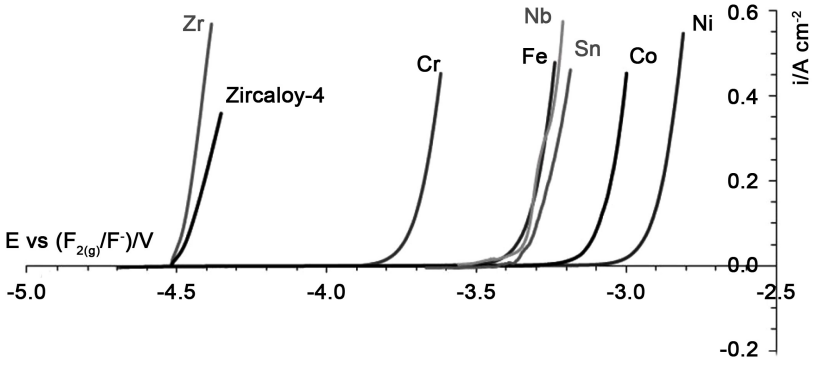

Figure 6. Comparison of linear voltammograms of oxidation of Zr, Cr, Fe, Nb, Sn, Co, Ni and Zircaloy-4 at 10 mV·s^{-1} in LiF-NaF at 750˚C.

Galvanostatic electrolyses were performed on Zircaloy-4 anodes in LiF-NaF at 750˚C. Cross-sections of the electrodes after electrolysis were characterized by SEM-EDS and a typical SEM micrograph obtained after electrolysis at −0.21 A·cm^{-2} during 1.1 h is presented in Figure 7. This micrograph evidences two zones: 1) a homogeneous area corresponding to the core of the anode which was not dissolved, and 2) a non-homogeneous degradation layer located at the surface of the anodes.

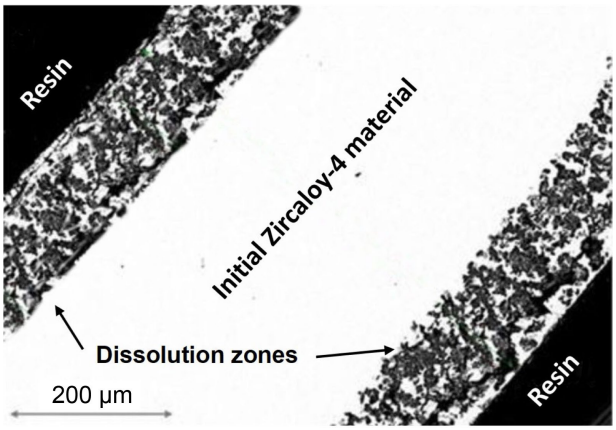

Figure 7. SEM observation of Zircaloy-4 anode cross-section after electrolysis in molten LiF-NaF at 750˚C and −0.21 A·cm^{-2} during 1.1 h.

The composition of the degradation layer was characterized by EDS analyses at different depths, from the surface to the core of the anode, as presented in Figure 8. This figure clearly evidences the two aeras observed in Figure 7. The composition of non-degraded Zircaloy-4 is homogeneous and identical to fresh material. In the degradation layer, Zr content is significantly lower than in the core of the anode while the content of other elements remains constant.

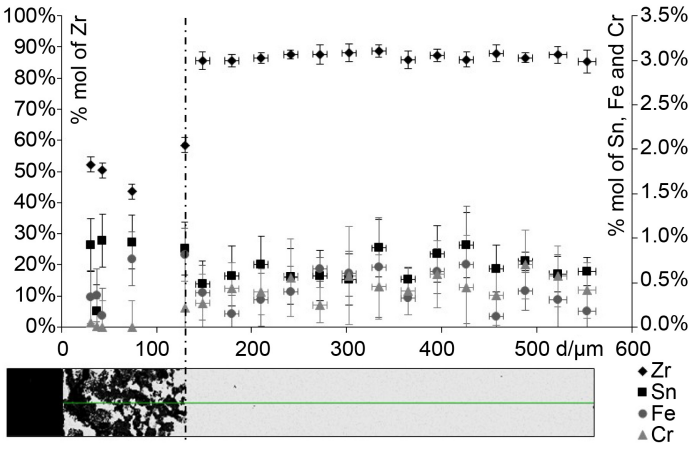

Figure 8. Concentration profiles of zirconium, tin, iron and chromium in Zircaloy-4 anode after electrolysis at −0.21 A·cm^{-2} for 1.1 h (Q = 1018 C) in LiF-NaF at 750˚C and SEM observation of electrolyzed Zircaloy-4 anode and location of the analysis profile lines.

The experiments were repeated for different durations, corresponding to a variation of anodic charge up to 2500 C. Similar morphologies of anodes were observed and the thickness of the degradation layer was plotted versus the anodic charge of the polarization (see Figure 9). A linear relationship was observed indicating that 1) only Zr was dissolved and 2) the anodic dissolution was not limited by intermetallic diffusion of Zr into Zircaloy-4.

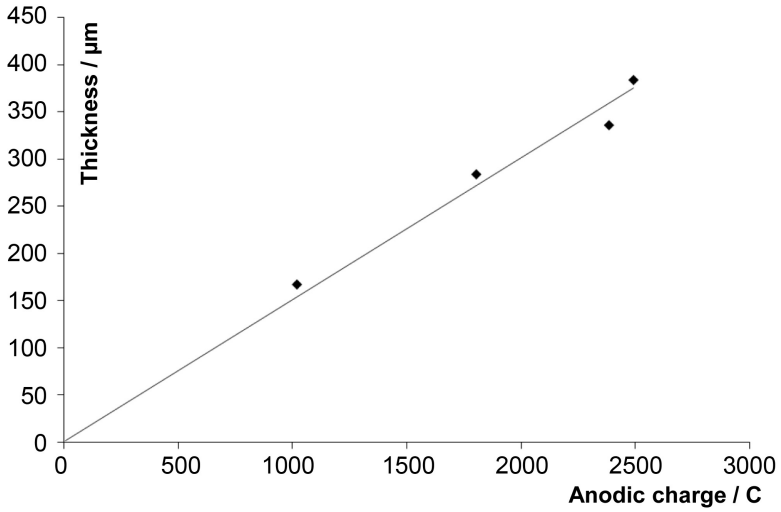

Figure 9. Zircaloy-4 degradation layer thickness versus anodic charge.

As Cr, Fe, Nb, Sn, Co and Ni are anodically dissolved at a higher potential than Zr, these results prove the selective dissolution of Zr from Zircaloy-4 anode. The strategy to selectively dissolve Zr at the anode and recover pure Zr at the cathode during electrorefining runs in this electrorefining is thus to control the oxidation potential.

3.4. Electrorefining

3.4.1. Electrorefining Progress

Five electrolyses corresponding to different electrical charges were performed at 750˚C in molten LiF-NaF-ZrF_4 (1.96 mol·kg^{-1}) with Zircaloy-4 as anode and graphite as cathode, and both anode and cathode potentials were recorded. A typical electrolysis record, plotting anode and cathode potentials and anode-cathode difference of potentials (ΔE) versus time is presented in Figure 10 for galvanostatic electrolysis at −0.15 A cm^{-2} during 3.2 hours. This figure highlights first that for duration lower than 4000 s, anode and cathode potentials similarly slightly increase while ΔE remains constant at around 0.15 V. This observation can be attributed to a small variation of the reference electrode potential. Then, in the 4000 - 8000 s duration range, all potentials remained stable. Finally, for $t > 8000$ s, cathode potential did not vary while anode potential sharply increased up to values higher than 0.5 V vs ($F_{2(g)}/F^-$). At this time, the electrolysis was immediately stopped to prevent impurities dissolution in the bath.

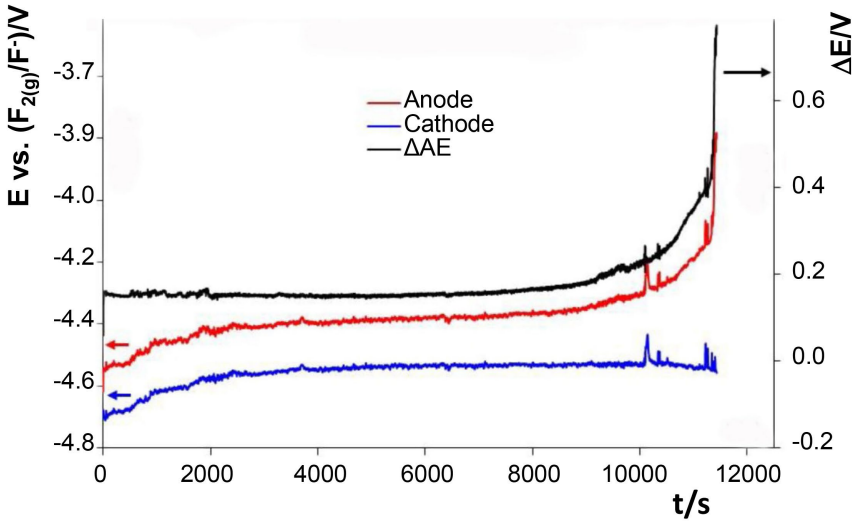

Figure 10. Typical variations of anodic (red), cathodic (blue) potentials and anode-cathode difference of potentials (black) during electrorefining run at −0.15 A·cm^{-2} during 3.1 hours in LiF-NaF-ZrF_4 (1.96 mol·kg^{-1}).

The dissolution progress can be calculated by weighting the anode before and after electrolysis (after salt cleaning) and the mass difference (Δm) is compared to the mass of Zr initially present in Zircaloy-4 anode immersed in the bath ($m_{i\,Zr}$) as follows:

$$\text{Dissolution progress} = \frac{\Delta m}{m_{i\,Zr}} \tag{8}$$

For electrolysis of **Figure 10**, the maximum dissolution progress of the anode without dissolving impurities was calculated at the end of electrolysis to be 74% in the case of the electrolysis presented in **Figure 10**.

The other key-points of the process are the purity of electrodeposited Zr, the anodic and cathodic faradic efficiencies.

3.4.2. Observations and Purities of Zr Deposits

At the end of the runs, both electrodes were cleaned and weighted. Photograph of the Zr deposits obtained after electrolysis runs are presented in **Figure 11**. In this figure, the growth of the coating clearly leads to big dendrites formation for a high quantity of Zr, confirming the conclusions provided in paragraph 3.2. If the dendrites are too brittle, they can be broken during the cleaning process, leading to a decrease in the recovery efficiency. However, it can be noted that no lack of dendrites can be observed on the deposits in **Figure 11**, meaning removing the salt from the deposit does not impact the metal recovery efficiency.

The deposits composition was analysed by SEM-EDS and the Zr, Sn, Fr and Cr content was measured (see **Table 2**). Only zirconium was detected by EDS, involving purity of the deposit higher than 99.9%. The content of other elements is thus lower than the limit of detection of EDS, estimated at 0.1%. In order to confirm that Sn, Fe and Cr were not dissolved during electrolyses, samples of the bath

were analysed, after cooling, by ICP-AES after several runs. The results show that Sn, Fe and Cr are effectively not detected in the bath, with a limit of quantification of 0.001 mass%. These results prove the high selectivity of Zr dissolution from Zircaloy-4.

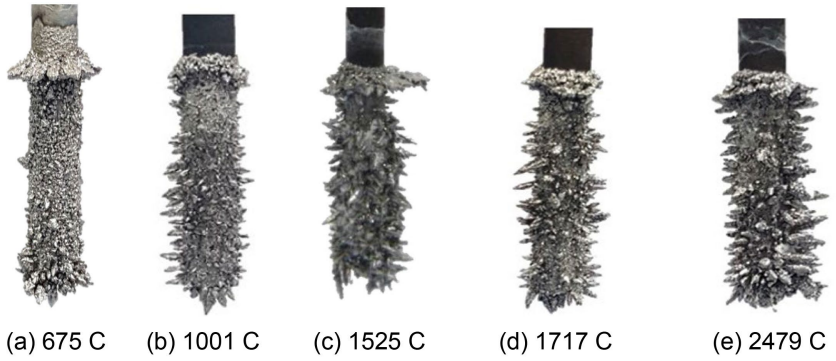

Figure 11. Photograph of Zr deposit obtained after electrorefining runs for different electrical charges at −0.14 A·cm^{-2} at 750˚C in molten LiF-NaF-ZrF_4 (1.96 mol·kg^{-1}).

Table 2. SEM-EDS analysis of Zr deposit obtained on graphite after electrorefining run at −0.14 A·cm^{-2} at 750˚C in molten LiF-NaF-ZrF_4 (1.96 mol·kg^{-1}).

Atomic %			
Zr	**Sn**	**Fe**	**Cr**
99.9%	<0.1%	<0.1%	<0.1%

3.4.3. Anodic and Cathodic Faradic Efficiencies

The mass variations of the anode and the cathode before and after electrolysis were measured and compared to the theoretical ones calculated from Faraday's law, considering only Zr dissolution and electrodeposition, allowing to calculate anodic and cathodic faradic efficiencies. All the results are summarized in **Table 3**.

Table 3. Anodic (Zircaloy-4) and cathodic (graphite) faradic efficiencies for electrorefining runs in molten LiF-NaF-ZrF_4 (1.93 mol·kg^{-1}) at 750˚C for various charges from 675 to 2479 C.

Q/C	Anodic faradic efficiency	Cathodic faradic efficiency
675	97% ± 3%	103% ± 3%
1001	98% ± 3%	99% ± 3%
1525	98% ± 3%	98% ± 3%
1717	98% ± 2%	108% ± 5%
2479	98% ± 2%	106% ± 3%

These results highlight that both anodic and cathodic faradic efficiencies are closed to 100%, in agreement with cathodic and anodic investigations. The obtained values higher than 100% can be attributed to the residual salt present in the

deposit after the cleaning process. Similar efficiencies were obtained in our laboratory concerning Si electrorefining from Si-Fe anodes [4]. All these results validate the electrorefining strategy developed during this study.

4. Conclusions

This work demonstrated that electrorefining is an efficient way for zirconium recovery from Zircaloy-4. Firstly, the influence of operating conditions on the morphology and adherence of Zr coating was investigated in molten LiF-NaF-ZrF_4 at 750˚C. In order to recover Zr, the best conditions are: the use of a graphite cathodic substrate, a high ZrF_4 concentration and a low applied current density. Then, the Zircaloy-4 anodic study evidenced a selective dissolution of Zr. The anodic and cathodic current efficiencies were estimated to be around 100% and the Zr deposits purity is assumed to be higher than 99.9%, as no other metal was detected in the deposit nor in the salt.

The plotting of anode and cathode potentials versus time during electrolysis evidenced a maximum dissolution progress of 74% to prevent impurities dissolution. This maximum progress can be directly monitored by cell voltage measurement as the main indicator to control the efficiency of electrorefining process. The maximum dissolution progress and faradic efficiencies are very promising results for Zircaloy-4 electrorefining process in molten fluorides. The next step of this study would be to evaluate electrorefining process efficiency directly from irradiated spent zircaloy-4 material obtained after a long stay in a nuclear reactor. In this case, Ziracloy-4 contains some activation products, fission products and actinides. The impact of these elements on the electrorefining strategy and performance has to be investigated.

Conflicts of Interest

The authors declare no conflicts of interest regarding the publication of this paper.

References

[1] Towner, R.R. (1992) International Strategic Minerals Inventory Summary Report. Zirconium, U.S. Department of the Interior, Geological Survey.

[2] Morize, P., Baicry, J. and Mardon, J. (1987) Effect of Irradiation at 588 K on Mechanical Properties and Deformation Behavior of Zirconium Alloy Strip. In: Adamson, R.B. and Van Swam, L.F.P., Eds., *Zirconium in the Nuclear Industry*, ASTM International, 101-119. https://doi.org/10.1520/stp28110s

[3] Whitmarsh, C.L. (1962) Review of Zircaloy-2 and Zircaloy-4 Properties Relevant to N. S. Savannah Reactor Design. Oak Ridge National Laboratory.

[4] Massot, L., Bieber, A.L., Gibilaro, M., Cassayre, L., Taxil, P. and Chamelot, P. (2013) Silicon Recovery from Silicon-Iron Alloys by Electrorefining in Molten Fluorides. *Electrochimica Acta*, **96**, 97-102. https://doi.org/10.1016/j.electacta.2013.02.065

[5] Ghosh, S., Vandarkuzhali, S., Venkatesh, P., Seenivasan, G., Subramanian, T., Prabhakara Reddy, B., *et al.* (2009) Electrochemical Studies on the Redox Behaviour of Zirconium in Molten LiCl-KCL Eutectic. *Journal of Electroanalytical Chemistry*, **627**,

15-27. https://doi.org/10.1016/j.jelechem.2008.12.011

[6] Lee, C.H., Kang, K.H., Jeon, M.K., Heo, C.M. and Lee, Y.L. (2012) Electrorefining of Zirconium from Zircaloy-4 Cladding Hulls in LiCl-KCL Molten Salts. *Journal of The Electrochemical Society*, **159**, D463-D468. https://doi.org/10.1149/2.012208jes

[7] Sakamura, Y. (2004) Zirconium Behavior in Molten LiCl-KCL Eutectic. *Journal of The Electrochemical Society*, **151**, C187. https://doi.org/10.1149/1.1644605

[8] Fabian, C.P., Luca, V., Le, T.H., Bond, A.M., Chamelot, P., Massot, L., *et al.* (2012) Cyclic Voltammetric Experiment—Simulation Comparisons of the Complex Mechanism Associated with Electrochemical Reduction of Zr^{4+}in LiCl-KCL Eutectic Molten Salt. *Journal of The Electrochemical Society*, **160**, H81-H86. https://doi.org/10.1149/2.016302jes

[9] Groult, H., Barhoun, A., El Ghallali, H., Borensztjan, S. and Lantelme, F. (2008) Study of the Electrochemical Reduction of Zr^{4+} Ions in Molten Alkali Fluorides. *Journal of The Electrochemical Society*, **155**, E19. https://doi.org/10.1149/1.2811848

[10] Gibilaro, M., Massot, L., Chamelot, P., Cassayre, L. and Taxil, P. (2013) Investigation of Zr(IV) in LiF-CaF_2: Stability with Oxide Ions and Electroreduction Pathway on Inert and Reactive Electrodes. *Electrochimica Acta*, **95**, 185-191. https://doi.org/10.1016/j.electacta.2013.02.022

[11] Xu, L., Xiao, Y., Xu, Q., van Sandwijk, A., Zhao, Z., Song, Q., *et al.* (2017) Electrochemical Studies on the Redox Behavior of Zirconium in the LiF-NaF Eutectic Melt. *Journal of Nuclear Materials*, **488**, 295-301. https://doi.org/10.1016/j.jnucmat.2017.03.028

[12] Xu, L., Xiao, Y., Xu, Q., van Sandwijk, A., Li, J., Zhao, Z., *et al.* (2016) Electrochemical Behavior of Zirconium in Molten LiF-KF-ZrF_4 at 600˚C. *RSC Advances*, **6**, 84472-84479. https://doi.org/10.1039/c6ra17102h

[13] Quaranta, D., Massot, L., Gibilaro, M., Mendes, E., Serp, J. and Chamelot, P. (2018) Zirconium(IV) Electrochemical Behavior in Molten LiF-NaF. *Electrochimica Acta*, **265**, 586-593. https://doi.org/10.1016/j.electacta.2018.01.213

[14] Han, W., Wang, W., Li, H., Zhao, Y., Wang, Y., Liu, R., *et al.* (2021) Electrochemical Recovering Zr from Molten Salt Using an Fe Electrode. *ACS Sustainable Chemistry & Engineering*, **9**, 17393-17402. https://doi.org/10.1021/acssuschemeng.1c06931

[15] Murakami, T. and Hayashi, H. (2022) Electrochemical Recovery of Zr and Cd from Molten Chloride Salts for Reprocessing of Used Nitride Fuels. *Journal of Nuclear Materials*, **558**, Article 153330. https://doi.org/10.1016/j.jnucmat.2021.153330

[16] Sohn, S., Park, J. and Hwang, I.S. (2018) Electrolytic Recovery of High Purity Zr from Radioactively Contaminated Zr Alloys in Chloride Salts. *International Journal of Electrochemical Science*, **13**, 3897-3909. https://doi.org/10.20964/2018.04.56

[17] Mamantov, G. (1969) Molten Salts: Characterization and Analysis. IOPScience.

[18] Bieber, A.L., Massot, L., Gibilaro, M., Cassayre, L., Taxil, P. and Chamelot, P. (2012) Silicon Electrodeposition in Molten Fluorides. *Electrochimica Acta*, **62**, 282-289. https://doi.org/10.1016/j.electacta.2011.12.039

[19] Massot, L., Chamelot, P., Palau, P. and Taxil, P. (2005) Electrocrystallisation of Tantalum in Molten Fluoride Media. *Electrochimica Acta*, **50**, 5408-5413. https://doi.org/10.1016/j.electacta.2005.03.021

[20] Chamelot, P., Taxil, P., Oquab, D., Serp, J. and Lafage, B. (2000) Niobium Electrodeposition in Molten Fluorides Using Pulsed Electrolysis. *Journal of The Electrochemical Society*, **147**, Article 4131. https://doi.org/10.1149/1.1394030